

DSCC2012-MOVIC2012-8782

PARAMETERIZATION AND VALIDATION OF AN INTEGRATED ELECTRO-THERMAL CYLINDRICAL LFP BATTERY MODEL

Hector E. Perez*
Jason B. Siegel
Xinfan Lin

Anna G. Stefanopoulou
Department of Mechanical Engineering
University of Michigan
Ann Arbor, Michigan 48109
Email: heperez@umich.edu

Yi Ding

Matthew P. Castanier
U.S. Army Tank Automotive
Research, Development,
and Engineering Center (TARDEC)
Warren, Michigan, 48397

ABSTRACT

In this paper, for the first time, an equivalent circuit electrical model is integrated with a two-state thermal model to form an electro-thermal model for cylindrical lithium ion batteries. The parameterization of such model for an A123 26650 LiFePO₄ cylindrical battery is presented. The resistances and capacitances of the equivalent circuit model are identified at different temperatures and states of charge (SOC), for charging and discharging. Functions are chosen to characterize the fitted parameters. A two-state thermal model is used to approximate the core and surface temperatures of the battery. The electrical model is coupled with the thermal model through heat generation and the thermal states are in turn feeding a radially averaged cell temperature affecting the parameters of the electrical model. Parameters of the thermal model are identified using a least squares algorithm. The electro-thermal model is then validated against voltage and surface temperature measurements from a realistic drive cycle experiment.

1 INTRODUCTION

Lithium Ion Batteries are attractive energy storage devices for Hybrid Electric (HEV), Plug In Hybrid Electric (PHEV), and Electric Vehicles (EV) due to their reasonable power and energy density. The ability to accurately predict the electrical and temperature dynamics of a battery is critical for designing onboard battery management systems (BMS), and thermal management systems.

Electrical models vary in complexity. For some applications, a simple model capturing the basic electrical behavior can be sufficient (eg. an OCV-R model). There are more complex electro-chemical models [1–3] that are highly accurate [4–6], but hard to be fully parameterized [6], and require large computational capacity. Therefore, they are not suitable for control oriented modeling. Equivalent circuit models are commonly used, which offer a tradeoff between accuracy and simplicity, and are suitable for control oriented applications [7–11].

The equivalent circuit model can capture the terminal voltage of the battery and has been widely adopted since the work in [12]. The voltage supply in the equivalent circuit, shown in Fig. 1, represents the open circuit voltage (V_{OCV}) which is a function of state of charge. The series resistance (R_s) represents internal resistance of the battery. The voltage drop across the two resistor-capacitor (RC) pairs (V_1 and V_2) are used to model the dynamic voltage losses due to lithium diffusion in the solid phase and in the electrolyte [13]. These circuit elements depend on state of charge (SOC), temperature, and current direction as shown in [10]. These parameter dependencies are important for accurately capturing the dynamics of battery terminal voltage throughout a usable range of temperature and state of charge.

In addition to predicting the terminal voltage, an accurate model of the battery temperature is needed for control and thermal management to constrain the operating temperature range. In common battery management systems (BMS), the battery temperature is often monitored to prevent over-heating. In applications with high power demands, such as automotive traction batteries, the internal temperature of the battery may rise quickly,

*Address all correspondence to this author.

due to joule heating, and can be higher than the surface temperature. However, in practice only the surface temperature of the battery may be measured. If only the surface temperature is used for safety monitoring, there exists the risk of over-heating. In addition, the degradation profile of lithium ion batteries is temperature dependent. The core temperature, which is closer to (if not exactly) the temperature of the electrode assembly, will provide a more accurate reference for the battery lifetime estimation in BMS. Therefore, a thermal model capable of predicting the core temperature is needed for battery thermal management.

Coupled electro-thermal models have been investigated using PDE based electrical models in [2, 4, 14], and equivalent circuit based electrical models in [15–18]. The thermal models used in these studies have either been complex, or very simple only capturing the lumped temperature. Complex thermal models that capture the detailed temperature distribution in a cell have been used [14, 19, 20], but require a large amount of computational resources, making them unsuitable for control oriented modeling. A simple thermal model that predicts the critical temperature of a cylindrical cell is desired, such as the two state thermal model that has been studied in [21, 22]. This model has the ability to capture the core temperature T_c of a cylindrical cell which is greater than the surface temperature T_s under high discharge rates [23]. The two state thermal model can be further expanded to a battery pack configuration to estimate unmeasured temperatures as presented in [22].

In this paper, for the first time, an OCV-R-RC-RC equivalent circuit electrical model is integrated with a two state thermal model to form an electro-thermal model for LFP batteries. Such model is valuable for onboard BMS capable of conducting both SOC estimation and temperature monitoring. In Section 2, the coupling between the heat generation and temperature in the integrated electro-thermal model is highlighted by the temperature dependence of the equivalent circuit parameters. In Section 3, we first show how the electrical model can be parameterized using a low current rate so that isothermal conditions could be assumed. The identified parameters and their dependencies on SOC, current direction, and temperature are examined. Basis functions are chosen to represent the temperature and SOC dependence of the circuit elements. Next the parameters of the thermal model are identified using the heat generation calculated by the modeled open circuit voltage for a high C-rate drive cycle. Finally in Section 4, the coupled electro-thermal model is validated against the measured terminal voltage and surface temperature data from a drive cycle experiment.

2 BATTERY MODEL

In this section the electrical and thermal battery models are presented. An OCV-R-RC-RC model is chosen to approximate the electrical dynamics, while a two-state thermal model is adopted to capture the core and surface temperatures of the battery. The model parameter dependencies are introduced, and an electro-thermal model is formed through a heat generation term.

2.1 Electrical Model

The battery state of charge (SOC) is defined by current integration as,

$$\dot{SOC} = -\frac{1}{3600C_n}I. \quad (1)$$

The nominal capacity of the cell $C_n(Ah)$ is found by cycling the battery cell per manufacturer recommendation [24]. The charging profile consists of a Constant Current - Constant Voltage (CC-CV) charging cycle that is terminated when the current tapers below 50mA, and the voltage at the end of discharge is 2.0 V. The battery electrical dynamics are modeled by an equivalent circuit as seen in Fig. 1. The double RC model structure is a good choice for this battery chemistry, as shown in [25]. The two RC pairs represent a slow and fast time constant for the voltage recovery as shown by,

$$\begin{aligned} \dot{V}_1 &= -\frac{1}{R_1C_1}V_1 + \frac{1}{C_1}I \\ \dot{V}_2 &= -\frac{1}{R_2C_2}V_2 + \frac{1}{C_2}I. \end{aligned} \quad (2)$$

The states V_1 and V_2 are the capacitor voltages. The parameters $R_1(\Omega), C_1(F)$ correspond to the first RC pair, and $R_2(\Omega), C_2(F)$ to the second RC pair. The states of the electrical model are SOC, V_1 , and V_2 . The current I is the input, and the model output is the battery terminal voltage V_T defined as,

$$V_T = V_{OCV} - V_1 - V_2 - IR_s, \quad (3)$$

where V_{OCV} represents the open circuit voltage, and R_s represents the internal resistance of the cell. The V_{OCV} curve is assumed to be the average of the charge and discharge curves taken at very low current ($C/20$), since the $LiFePO_4$ cell chemistry is known to yield a hysteresis effect as shown in [25, 26]. This phenomena has been modeled for NiMH and lithium ion cells [25–29], but will be neglected in this study. The open circuit voltage V_{OCV} depends only on SOC; however, the equivalent circuit parameters depend on SOC, temperature, and current direction as shown in [10] and the results of this paper.

The cell temperature is driven by heat generation $Q(W)$ defined as,

$$Q = I(V_{OCV} - V_T). \quad (4)$$

The heat generation Q in the battery cell is defined by the polarization heat from joule heating and energy dissipated in the electrode over-potentials [19]. The effect of the entropic heat generation is excluded for simplicity, as it is relatively small compared to the total heat generation for an $LiFePO_4$ cell as shown by [23]. The entropic heat would contribute less than 1% of mean Q for the drive cycle used in this paper.

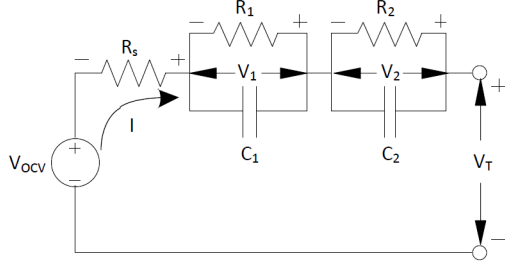


Figure 1. SINGLE CELL EQUIVALENT CIRCUIT MODEL.

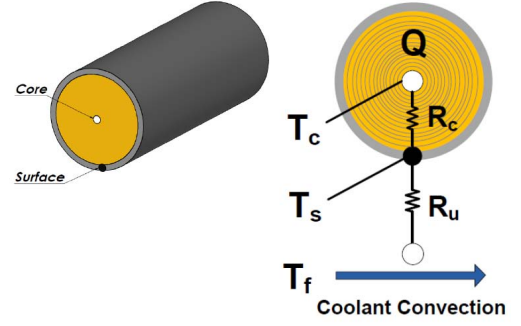


Figure 2. CELL LUMPED PARAMETER THERMAL MODEL WITH TWO STATES REPRESENTING THE CORE AND THE SURFACE TEMPERATURE.

2.2 Thermal Model

The radial temperature distribution inside a cylindrical battery can be described by PDEs based on the heat generation and transfer. Here, a simplified two state thermal model is defined as

$$\begin{aligned} C_c \dot{T}_c &= Q + \frac{T_s - T_c}{R_c} \\ C_s \dot{T}_s &= \frac{T_f - T_s}{R_u} - \frac{T_s - T_c}{R_c}, \end{aligned} \quad (5)$$

where $T_c(^{\circ}C)$ and $T_s(^{\circ}C)$ represent the core and surface temperature states respectively. The temperature used by the equivalent circuit model is the mean of the core and surface temperatures defined as $T_m(^{\circ}C)$,

$$T_m = \frac{T_s + T_c}{2}. \quad (6)$$

The inputs are the inlet air coolant temperature $T_f(^{\circ}C)$ and the heat generation Q calculated by the electrical model shown by Eq. 4. The parameters $C_c(J/K)$ and $C_s(J/K)$ are the lumped heat capacities of the core and surface respectively, $R_c(K/W)$ is the equivalent conduction resistance between the core and surface of the cell, and $R_u(K/W)$ is the equivalent convection resistance around the cell. The convective resistance R_u depends on the flow condition, and can be modeled for different types of coolants as described in [30, 31].

2.3 Model Coupling

The electro-thermal model is formed by taking the calculated heat generation from the electrical model as an input to the thermal model. The thermal model then generates the battery surface and core temperatures, used to find the mean battery temperature for the parameters of the electrical model, as shown in Fig. 3. The inputs of the electro-thermal model are the current I for the electrical model, and the air inlet temperature T_f for the thermal model. The electro-thermal model outputs are SOC, voltage, and the battery temperatures.

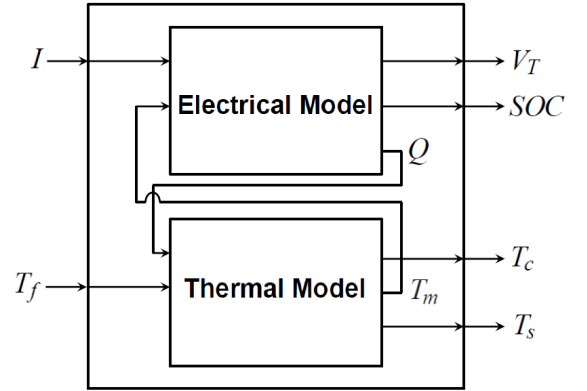


Figure 3. ELECTRO-THERMAL MODEL DIAGRAM.

The coupling results in a negative feedback, which can be seen from the temperature dependence of the battery internal resistance. To understand this coupling, consider a constant current. Under this condition the heat generation Q will decrease when cell temperature increases, because the reaction kinetics become more favorable, which further reduces the internal resistance. More rigorous stability analysis can be done with small signal analysis after linearization, although nonlinear tools will be needed for full understanding of the dynamical coupled system.

3 MODEL PARAMETER IDENTIFICATION

In this section the electrical and thermal model parameterization methods are described. First the parameters of the equivalent circuit model are identified from pulse current discharge/charge and relaxation experiments at different SOC's and temperatures with the battery placed inside a thermal chamber. Then using the calculated heat generation of the cell, the parameterization of the thermal model is presented using a least-squared fitting algorithm originally developed in [32].

There are different methods of identifying equivalent circuit model parameters such as electro impedance spectroscopy (EIS) [11], genetic algorithm (GA) optimization [25], and nonlinear least squares curve fitting techniques [10]. Most of these involve identifying parameters with respect to SOC as in [7–9, 11, 33], in addition the parameters are shown to depend on temperature and current direction [10, 15, 25]. The method selected here is to identify parameters from experimental pulse current data using nonlinear least squares curve fitting. Assuming isothermal conditions the identification is performed at each temperature and SOC grid point (5 parameters per pulse) in order to avoid simultaneous identification of the full parameter set (ie. 360 parameters in this model). This reduces the computational burden and allows us to investigate the equivalent circuit's parameter dependence on temperature and SOC.

3.1 Electrical Model Parameterization

Experiments to parameterize the electrical model for a 2.3Ah A123 26650 *LiFePO₄* cell were conducted using a Yokogawa GS-610 Source Measure Unit to control the current, and a Cincinnati Sub-Zero ZPHS16-3.5-SCT/AC environmental chamber to regulate the air coolant temperature. The tests were conducted in the environmental chamber. The battery temperature is assumed to be isothermal and T_m equal to the ambient temperature in the chamber due to the low C-rate experiments. This assumption is consistent with the small measured rise in surface temperature of the battery cell, less than 0.7°C, during the pulsed discharge.

First the capacity of the cell is measured by cycling the battery at low rate ($C/20$). The V_{OCV} curve is assumed to be the average of the charge/discharge curves corresponding to the same $C/20$ cycle test at 25°C. The effect of hysteresis in this cell chemistry results in a voltage gap between the charge and discharge curves as explained in [25–28]. Since hysteresis is not being modeled in this paper, the average curve is used for V_{OCV} . It is shown in [10], that there is a minimal effect on V_{OCV} with respect to the temperature range of study here for an *LiFePO₄* cell. Therefore, V_{OCV} is modeled with an SOC dependence.

After V_{OCV} and capacity are determined, the experiments to generate data for parameterization of the RC elements are conducted. First the cell sits at a constant temperature set point for 2h to ensure thermal equilibrium. The battery is then charged up to 100% SOC using a 1C CC-CV charge protocol at the 3.6V maximum until a 50mA CV cutoff current is reached. It is then discharged by 10%SOC at 1C rate, and relaxed for 2h. This process is repeated until the 2V minimum is reached. The pulse current followed by a 2h relaxation profile is repeated for the charge direction up to the 3.6V maximum. The pulse discharging and charging is conducted at different temperatures, resulting in 15°C, 25°C, 35°C, 45°C datasets. The voltage and current profile of one of the pulse discharge tests at 15°C is shown in Fig. 4.

The equivalent circuit parameter $R_s(\Omega)$ is found using

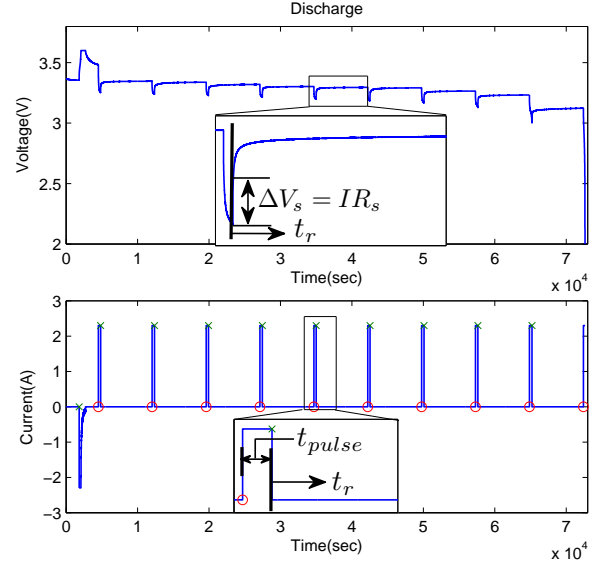


Figure 4. PULSE DISCHARGE VOLTAGE AND CURRENT PROFILE.

Ohm's law and the measured initial voltage jump ΔV_s (shown in the inset of the top subplot of Fig. 4) defined as,

$$R_s = \frac{\Delta V_s}{I}, \quad (7)$$

where I is the current applied during the pulse discharge/charge before the relaxation period (eg. 2.3A as shown in the inset of the bottom subplot of Fig. 4). The remaining equivalent circuit model parameters are identified by minimizing the error in voltage between the model and data during the relaxation period,

$$J_{Electrical} = \min \sum_{i=1}^n (V_{relax}(i) - V_{T,data}(i))^2, \quad (8)$$

using the lsqcurvefit function in MATLAB. Each instance is represented by i , starting from the first voltage relaxation datapoint $i = 1$, up to the last datapoint $i = n$.

The voltage recovery during relaxation, $V_{relax}(t_r)$, is derived by solving Eq. (2), assuming the capacitor voltages V_1, V_2 at the end of the previous rest period are zero

$$V_{relax}(t_r) = IR_1(1 - \exp(-\frac{t_{pulse}}{R_1C_1}))(1 - \exp(-\frac{t_r}{R_1C_1})) + IR_2(1 - \exp(-\frac{t_{pulse}}{R_2C_2}))(1 - \exp(-\frac{t_r}{R_2C_2})) + IR_s, \quad (9)$$

where t_{pulse} is duration of the constant current pulse prior to the relaxation period, and t_r is the time since the start of relaxation, as shown in Fig. 4. The parameters to be fitted are $R_1, R_2, C_1,$ and C_2 , and R_s is calculated by Eq. (7).

The inclusion of two or more RC pairs in the equivalent circuit model increases the accuracy of the cell voltage dynamic prediction as seen in [7, 9, 11, 25]. A comparison of the performance for best fit single RC, double RC, and triple RC models is shown Fig. 5. One can see that the single RC pair model yields large error especially during the first 500 seconds of relaxation, whereas the double RC and triple RC pair models yield less error across the entire dataset time period. It is evident that the higher order RC models can achieve a better fit to the relaxation voltage data than that of the single RC pair model. Furthermore, comparing with the fitting results using a double RC model, limited improvement in voltage fitting is observed when a triple RC model is applied, which potentially indicates an overparameterization. Consequently, the double RC pair model is the appropriate choice.

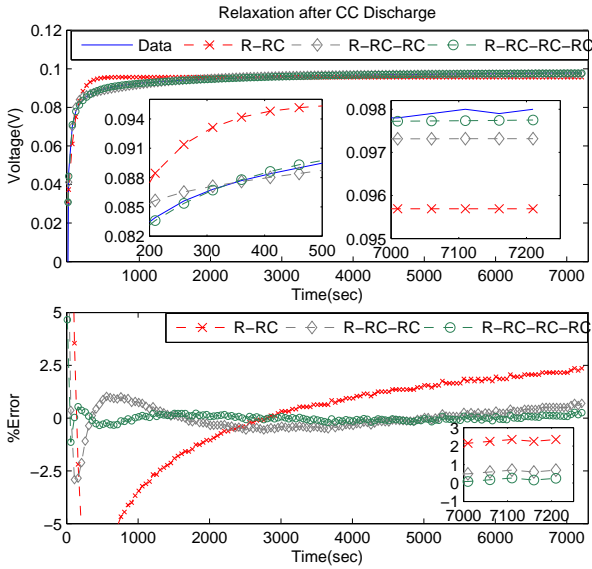


Figure 5. FITTING OF VOLTAGE RELAXATION DATA.

3.2 Equivalent Circuit Parameters

The equivalent circuit parameters can then be characterized as functions of SOC, and temperature for the discharge and charge direction as shown in [10]. The calculated internal resistance R_s from Eq. (7), is shown in Fig. 6 with respect to SOC and temperature for discharge and charge. The internal resistance R_s has a minimal dependence on SOC over the range of 10 to 90 %, but depends strongly on temperature and current direction. Therefore, the R_s parameter can be represented by an exponential function of the mean temperature T_m , for the discharging and

charging cases, as shown by,

$$R_s = \begin{cases} R_{s_d}, & I \geq 0 \text{ (discharge)} \\ R_{s_c}, & I < 0 \text{ (charge)} \end{cases} \quad (10)$$

$$R_{s_*} = R_{s0_*} \exp\left(\frac{T_{ref} R_{s_*}}{T_m - T_{shift} R_{s_*}}\right),$$

where $*$ = d, c represents the value during discharging and charging respectively. The characterized R_s functions in Eq. (10) are plotted along with the R_s values fit from the relaxation data using Eq. (8), in Fig. 6. The values for Eq. (10) are shown in Tab. 1.

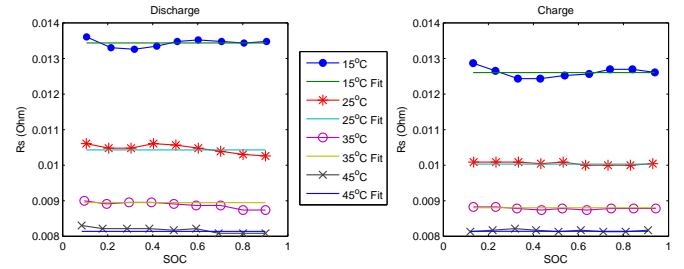


Figure 6. CALCULATED R_s VERSUS PARAMETRIC FUNCTIONS DESCRIBING THEIR DEPENDENCE ON TEMPERATURE AND SOC.

Table 1. PARAMETRIC R_s FUNCTION PARAMETERS.

| R_{s0d} | R_{s0c} | $T_{ref} R_{s_d}$ | $T_{ref} R_{s_c}$ | $T_{shift} R_{s_d}$ | $T_{shift} R_{s_c}$ |
|-----------|-----------|-------------------|-------------------|---------------------|---------------------|
| 0.0048 | 0.0055 | 31.0494 | 22.2477 | -15.3253 | -11.5943 |

The parameters R_1, R_2 are characterized by including an SOC dependency to the function in Eq. (10) used for the parameter R_s . The corresponding R_1, R_2 functions including SOC and temperature dependence for discharge and charge are shown in Eq. (19) and Eq. (20). The characterized functions are plotted along with the R_1, R_2 parameter values in Fig. 11 and Fig. 12.

The parameters C_1, C_2 are represented by polynomial SOC functions including temperature dependence. The C_1, C_2 functions including SOC and temperature dependence for discharge and charge are shown in Eq. (21) and Eq. (22). They are plotted along with the C_1, C_2 parameter values in Fig. 13 and Fig. 14.

3.3 Thermal Model Parameterization

The experiment procedure used to identify the thermal model parameters is the Urban Assault Cycle (UAC), scaled for the A123 26650 cell, as explained in [32]. This cycle has been presented in [34], for a 13.4 ton armored military vehicle. The

cell is first charged to 100%SOC using a 1C CC-CV protocol until the 50mA CV cutoff current is reached. It is then discharged at 1C to about 50%SOC. The UAC current profile is then applied to the cell under constant coolant flow, with the measured inlet temperature T_f as shown in Fig. 7.

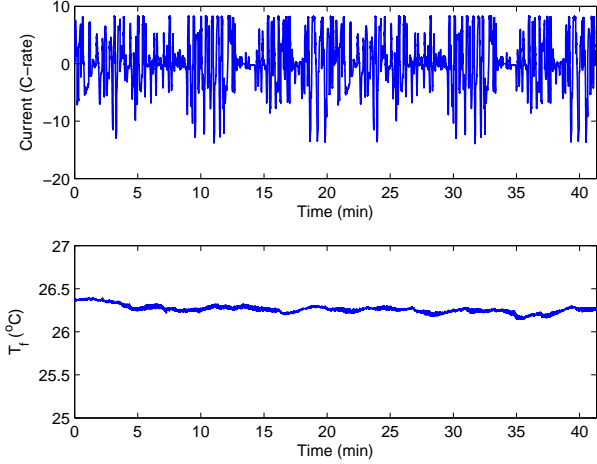


Figure 7. UAC CURRENT AND INLET TEMPERATURE PROFILE.

The experiment is done by using a Bitrode FTV1-200/50/2-60. The battery cell is placed in a designed flow chamber as shown in Fig. 8, where a Pulse Width Modulated (PWM) fan is mounted at the end to regulate the air flow rate around the cell. This flow chamber is used to emulate cooling conditions of a cell in a pack, where the flowrate is adjustable. Two T-type thermocouples are used for temperature measurement, one attached to the aluminum casing of the cell to measure the surface temperature T_s , and the other near the battery inside the flow chamber to measure the air flow temperature T_f . This thermal identification experiment setup is also presented in [32].

The non-recursive least squares thermal model identification method described in [22, 32] is implemented here by using the heat generation from Eq. (4) as the input for the thermal model, where V_T is the measured voltage, V_{OCV} is the modeled open circuit voltage, and I is the measured current. The objective is to minimize the sum of the squared errors between the the modeled surface temperature T_s , and the measured surface temperature $T_{s,data}$ as shown by the cost function,

$$J_{Thermal} = \min \sum_{i=1}^n (T_s(i) - T_{s,data}(i))^2, \quad (11)$$

where each instance is represented by i , starting from the first surface temperature datapoint $i = 1$, up to the last datapoint $i = n$.

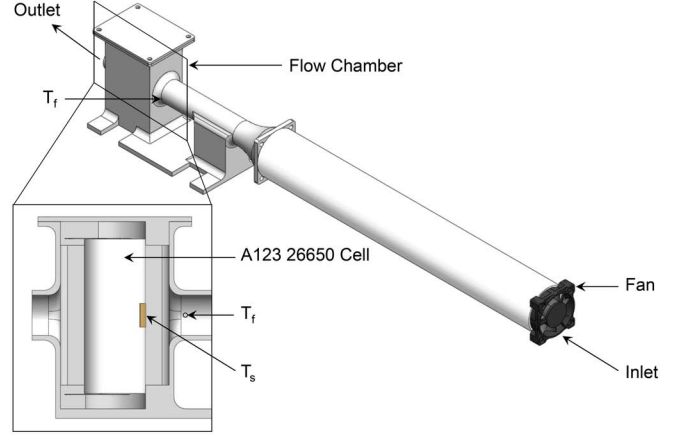


Figure 8. SINGLE CELL FLOW CHAMBER.

A parametric model in the form of [35],

$$z = \theta^T \phi, \quad (12)$$

is used for the thermal model parameter least squares identification [22], where the observation z and the independent regressors ϕ should be measured. The parameters in θ are calculated by the non-recursive least squares after the experimental data is taken over a period of time t_1, t_2, \dots, t by [35],

$$\begin{aligned} \theta(t) &= (\Phi^T(t)\Phi(t))^{-1} \Phi(t)Z(t), \\ Z(t) &= \begin{bmatrix} \frac{z(t_1)}{m(t_1)} & \frac{z(t_2)}{m(t_2)} & \dots & \frac{z(t)}{m(t)} \end{bmatrix}^T \\ \Phi(t) &= \begin{bmatrix} \frac{\phi^T(t_1)}{m(t_1)} & \frac{\phi^T(t_2)}{m(t_2)} & \dots & \frac{\phi^T(t)}{m(t)} \end{bmatrix}^T \\ m(t) &= \sqrt{1 + \phi^T(t)\phi(t)}, \end{aligned} \quad (13)$$

where $m(t)$ is the normalization factor to enhance the robustness of parameter identification as explained in [22]. For this purpose, the parametric model for the linear model identification with initial battery surface temperature condition $T_{s,0}$ is first derived. The thermal model in Eq. (5) becomes [22],

$$\begin{aligned} s^2 T_s - s T_{s,0} &= \frac{1}{C_c C_s R_c} Q + \frac{1}{C_c C_s R_c R_u} (T_f - T_s) \\ &\quad - \left(\frac{C_c + C_s}{C_c C_s R_c} + \frac{1}{C_s R_u} \right) (s T_s - T_{s,0}), \end{aligned} \quad (14)$$

after a Laplace transformation and substitution of the unmeasurable T_c by the measurable T_f, T_s . To avoid using the derivatives

Table 2. THERMAL MODEL PARAMETERS.

| $C_s(J/K)$ | $C_c(J/K)$ | $R_c(K/W)$ | $R_u(K/W)$ |
|------------|------------|------------|------------|
| 4.5 | 62.7 | 1.94 | 3.19 |

of the measured signals, a proper parametric model must be obtained. For this purpose, a second order filter is designed and applied to the parametric model in Eq. (12),

$$\frac{z}{\Lambda} = \theta^T \frac{\phi}{\Lambda}, \quad (15)$$

where the observation z and the independent regressors ϕ are measured. The time constants of the filter can be determined based on analyzing the persistent excitation condition for online parameterization under typical drive cycles [22]. The parameter vector θ is defined as,

$$\begin{aligned} z &= s^2 T_s - s T_{s,0} \\ \phi &= [Q \ T_f - T_s \ s T_s - T_{s,0}]^T \\ \theta &= [\alpha \ \beta \ \gamma]^T, \end{aligned} \quad (16)$$

where the parameters α, β, γ are,

$$\alpha = \frac{1}{C_c C_s R_c}, \quad \beta = \frac{1}{C_c C_s R_c R_u}, \quad \gamma = -\left(\frac{C_c C_s}{C_c C_s R_c} + \frac{1}{C_s R_u}\right). \quad (17)$$

By applying the parameterization algorithm, α, β and γ can be identified. It is clear that only three out of the four parameters (C_c, C_s, R_c and R_u) can be determined by solving Eq. (17). Hence C_s is pre-calculated based on the specific heat capacity and dimensions of the aluminum casing. With C_s known, C_c, R_u , and R_c can be calculated by

$$R_u = \frac{\alpha}{\beta}, \quad R_c = \frac{1}{\beta C_s C_c R_u}, \quad C_c = \frac{1}{\alpha C_s R_c}. \quad (18)$$

The resulting identified parameters C_c, R_c and R_u from the thermal identification scheme are shown in Tab. 2. The parameters C_c, C_s, R_c should not change significantly within the lifetime of the battery cell due to their physical properties. The parameter R_u can change with respect to the flow around the cell as previously mentioned. In this case it is identified as a constant for a steady flow condition.

4 MODEL VALIDATION AND RESULTS

The electro-thermal model is implemented in Simulink to validate its performance under the UAC experiment. The SOC,

temperature, and current direction dependencies of the equivalent circuit model parameters are included using lookup tables. The current I and air inlet temperature T_f inputs are shown in Fig. 7. The voltage and temperature responses of the electro-thermal model are compared to the experimental measurements. SOC is shown in Fig. 9 for this experiment. The SOC varies

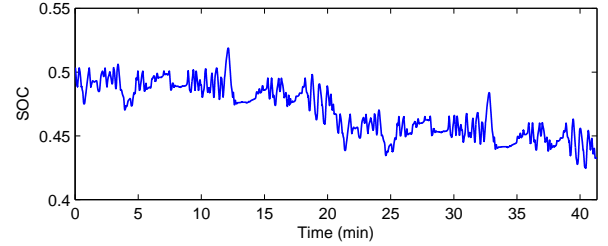


Figure 9. UAC SIMULATION SOC RESULTS.

between 52% and 42% under these conditions.

The measured surface temperature $T_{s,data}$ and terminal voltage $V_{T,data}$, are compared to the predicted surface temperature T_s and voltage V_T as shown in Fig. 10. The root mean square error (RMSE) in predicted surface temperature is $0.32^\circ C$ and voltage is 19.3mV. The voltage RMSE is comparable with published results in [29], using a similar type of drive cycle profile for this type of cell. The predicted core temperature T_c is also shown in Fig. 10, which is $2.78^\circ C$ higher than the predicted surface temperature T_s under this cycle. A higher T_c prediction is presented in [32], using a different heat generation under the same experimental conditions. The heat generation for our case is smaller than [32], causing slightly different identified parameters and a lower T_c prediction. Further investigation is required to determine if the calculated heat generation Q and core temperature T_c prediction are correct. Including a hysteresis model in the electro-thermal model will also need to be investigated to determine if better results can be achieved.

5 CONCLUSION AND FUTURE WORK

In this study an equivalent circuit electrical model along with a two state thermal model for an A123 26650 $LiFePO_4$ cell were parameterized. The models were integrated into an electro-thermal model in MATLAB/Simulink through a coupling heat generation and temperature feedback. The resulting electro-thermal model matches experimental measurements with minimal error. This shows that the parameterization schemes used are adequate for battery modeling.

Future work will involve modeling of hysteresis as in [25, 27, 28], which will then cause the heat generation to change due to the new V_{OCV} term. Measurement of the core temperature T_c is also planned to validate the core temperature estimation of the electro-thermal model. The cylindrical battery is to be drilled

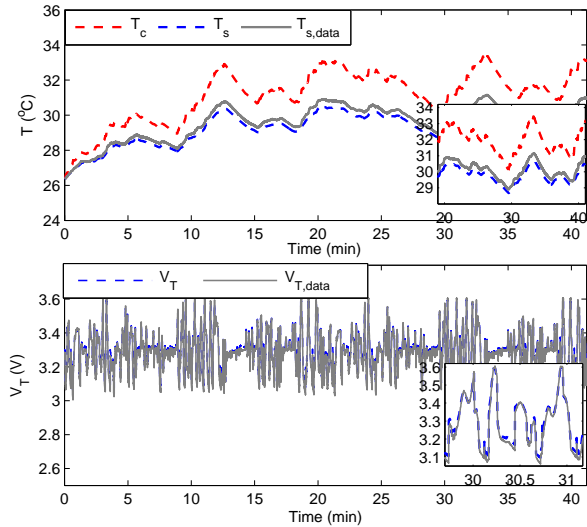


Figure 10. UAC TEMPERATURE AND VOLTAGE RESULTS.

and a thermocouple will be installed in the core of the battery to measure the core temperature as in [23].

ACKNOWLEDGMENT

Thanks go to the U.S. Army Tank Automotive Research, Development, and Engineering Center (TARDEC), and Automotive Research Center (ARC), a U.S. Army center of excellence in modeling and simulation of ground vehicles, for providing support including funding. UNCLASSIFIED: Distribution Statement A. Approved for public release.

REFERENCES

- [1] Fuller, T. F., Doyle, M., and Newman, J., 1994. "Simulation and optimization of the dual lithium ion insertion cell". *Journal of the Electrochemical Society*, **141**(1), January, pp. 1–10.
- [2] Gu, W. B., and Wang, C. Y., 2000. "Thermal and electrochemical coupled modeling of a lithium-ion cell". In *Lithium Ion Batteries*, ECS Proceedings.
- [3] Wang, C. Y., Gu, W. B., and Liaw, B. Y., 1998. "Micro-macroscopic coupled modeling of batteries and fuel cells i. model development". *Journal of the Electrochemical Society*, **145**(10), October, pp. 3407–3417.
- [4] Fang, W., Kwon, O. J., and Wang, C. Y., 2010. "Electrochemical-thermal modeling of automotive li-ion batteries and experimental validation using a three-electrode cell". *International Journal of Energy Research*, **34**(2), February, pp. 107–115.
- [5] Speltino, C., Domenico, D. D., Fiengo, G., and Stefanopoulou, A., 2009. "On the experimental identification and validation of an electrochemical model of a lithium-ion battery". In *American Control Conference*.
- [6] Forman, J. C., Moura, S. J., Stein, J. L., and Fathy, H. K., 2011. "Genetic parameter identification of the doyle-fuller-newman model from experimental cycling of a lifepo4 battery". In *American Control Conference (ACC)*, 2011.
- [7] Chen, M., and Rincon-Mora, G. A., 2006. "Accurate electrical battery model capable of predicting runtime and i-v performance". *IEEE Transactions on Energy Conversion*, **21**(2), June, pp. 504–511.
- [8] Knauff, M., McLaughlin, J., Dafis, C., Nieber, D., Singh, P., Kwatny, H., and Nwankpa, C., 2010. "Simulink model of a lithium-ion battery for the hybrid power system testbed". In *Proceedings of the ASNE Intelligent Ships Symposium*.
- [9] Einhorn, M., Conte, V., Kral, C., and Fleing, J., 2011. "Comparison of electrical battery models using a numerically optimized parameterization method". In *Proceedings of the IEEE Vehicle Power and Propulsion Conference (VPPC)*, 2011 IEEE.
- [10] Lam, L., Bauer, P., and Kelder, E., 2011. "A practical circuit-based model for li-ion battery cells in electric vehicle applications". In *Proceedings of 33rd IEEE International Telecommunications Energy Conference INTELEC 2011*.
- [11] Dubarry, M., and Liaw, B. Y., 2007. "Development of a universal modeling tool for rechargeable lithium batteries". *Journal of Power Sources*, **174**(2), December, pp. 856–860.
- [12] Salameh, Z. M., Casacca, M. A., and Lynch, W. A., 1992. "A mathematical model for lead-acid batteries". *IEEE Transactions on Energy Conversion*, **7**(1), March, pp. 93–97.
- [13] Smith, K. A., 2006. "Electrochemical modeling, estimation and control of lithium ion batteries". PhD Thesis, Pennsylvania State University, University Park, PA, December.
- [14] Wang, C. Y., and Srinivasan, V., 2002. "Computational battery dynamics (cbd)-electrochemical/thermal coupled modeling and multi-scale modeling". *Journal of Power Sources*, **110**(2), August, pp. 364–376.
- [15] Smith, K., Kim, G., Darcy, E., and Pesaran, A., 2010. "Thermal/electrical modeling for abuse-tolerant design of lithium ion modules". *International Journal of Energy Research*, **34**(2), February, pp. 204–215.
- [16] Gao, L., Liu, S., and Dougal, R., 2002. "Dynamic lithium-ion battery model for system simulation". *IEEE Transactions on Components and Packaging Technologies*, **25**(3), September, pp. 495–505.
- [17] Huria, T., Ceraolo, M., Gazzari, J., and Jackey, R., 2012. "High fidelity electrical model with thermal dependence for characterization and simulation of high power lithium battery cells". In *2012 IEEE International Electric Vehicle Conference*.
- [18] Benger, R., Wenzl, H., Beck, H. P., Jiang, M., Ohms, D., and Schaedlich, G., 2009. "Electrochemical and thermal modeling of lithium-ion cells for use in hev or ev application". *World Electric Vehicle Journal*, **3**(ISSN 2032-6653), May, pp. 1–10.

[19] Bernardi, D., Pawlikowski, E., and Newman, J., 1985. "A general energy balance for battery systems". *Journal of the Electrochemical Society*, **132**(1), January, pp. 5–12.

[20] Hallaj, S. A., Maleki, H., Hong, J. S., and Selman, J. R., 1999. "Thermal modeling and design considerations of lithium-ion batteries". *Journal of Power Sources*, **83**(1-2), October, pp. 1–8.

[21] Park, C., and Jaura, A. K., 2003. "Dynamic thermal model of li-ion battery for predictive behavior in hybrid and fuel cell vehicles". In SAE 2003-01-2286.

[22] Lin, X., Perez, H. E., Siegel, J. B., Stefanopoulou, A. G., Ding, Y., and Castanier, M. P., 2011. "Parameterization and observability analysis of scalable battery clusters for onboard thermal management". In Proceedings of International scientific conference on hybrid and electric vehicles RHEVE 2011.

[23] Forgez, C., Do, D. V., Friedrich, G., Morcrette, M., and Delacourt, C., 2010. "Thermal modeling of a cylindrical lifepo4/graphite lithium-ion battery". *Journal of Power Sources*, **195**(9), May, pp. 2961–2968.

[24] A123Systems Inc., 2006. A123 systems datasheet: High power lithium ion anr26650m1. www.a123systems.com.

[25] Hu, Y., Yurkovich, B. J., Yurkovich, S., and Guezennec, Y., 2009. "Electro-thermal battery modeling and identification for automotive applications". In Proceedings of 2009 ASME Dynamic Systems and Control Conference DSCC.

[26] Roscher, M. A., and Sauer, D. U., 2011. "Dynamic electric behavior and open-circuit-voltage modeling of lifepo4-based lithium ion secondary batteries". *Journal of Power Sources*, **196**(1), January, pp. 331–336.

[27] Verbrugge, M., and Tate, E., 2004. "Adaptive state of charge algorithm for nickel metal hydride batteries including hysteresis phenomena". *Journal of Power Sources*, **126**(12), February, pp. 236–249.

[28] Plett, G. L., 2004. "Extended kalman filtering for battery management systems of lipb-based hev battery packs part 2. modeling and identification". *Journal of Power Sources*, **134**(2), August, pp. 262–276.

[29] Hu, Y., Yurkovich, S., Guezennec, Y., and Yurkovich, B. J., 2011. "Electro-thermal battery model identification for automotive applications". *Journal of Power Sources*, **196**(1), January, pp. 449–457.

[30] Zukauskas, A., 1972. "Heat transfer from tubes in cross-flow". *Advances in Heat Transfer*, **18**, pp. 93–160.

[31] Lin, X., Perez, H. E., Siegel, J. B., Stefanopoulou, A. G., Li, Y., and Anderson, R. D., 2012. Quadruple adaptive observer of li-ion core temperature in cylindrical cells and their health monitoring. In 2012 American Control Conference (Accepted).

[32] Lin, X., Perez, H. E., Siegel, J. B., Stefanopoulou, A. G., Li, Y., Anderson, R. D., Ding, Y., and Castanier, M. P., 2012. On-line parameterization of lumped thermal dynamics in cylindrical lithium ion batteries for core temperature estimation and health monitoring. Submitted to the 2012

IEEE Transactions on Control System Technology Journal, January.

[33] Liaw, B. Y., Nagasubramanian, G., Jungst, R. G., and Doughty, D. H., 2004. "Modeling of lithium ion cells—a simple equivalent-circuit model approach". *Solid State Ionics*, **175**(1-4), November, pp. 835–839.

[34] Lee, T. K., Kim, Y., Stefanopoulou, A., and Filipi, Z. S., 2011. "Hybrid electric vehicle supervisory control design reflecting estimated lithium-ion battery electrochemical dynamics". In 2011 American Control Conference (ACC).

[35] Ioannou, P. A., and Sun, J., 1996. *Robust Adaptive Control*. Prentice Hall.

Appendix: Calculated Parameters and Functions

$$R_1 = \begin{cases} R_{1d}, & I \geq 0 \text{ (discharge)} \\ R_{1c}, & I < 0 \text{ (charge)} \end{cases}$$

$$R_{1*} = (R_{10*} + R_{11*}(SOC) + R_{12*}(SOC)^2) \exp\left(\frac{T_{ref}R_{1*}}{T_m - T_{shift}R_{1*}}\right) \quad (19)$$

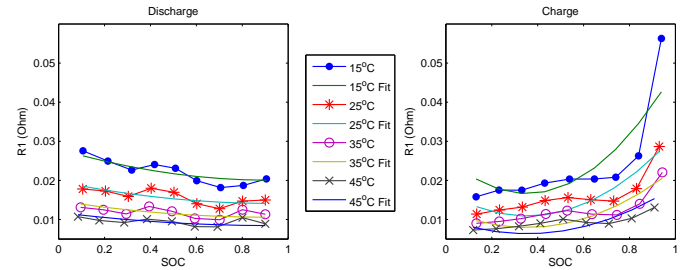


Figure 11. CALCULATED R_1 VERSUS PARAMETRIC FUNCTIONS DESCRIBING THEIR DEPENDENCE ON TEMPERATURE AND SOC.

Table 3. PARAMETRIC R_1 FUNCTION PARAMETERS.

| R_{10d} | R_{10c} | R_{11d} | R_{11c} | R_{12d} |
|-----------|-----------------|-----------------|-------------------|-------------------|
| 7.1135e-4 | 0.0016 | -4.3865e-4 | -0.0032 | 2.3788e-4 |
| R_{12c} | $T_{ref}R_{1d}$ | $T_{ref}R_{1c}$ | $T_{shift}R_{1d}$ | $T_{shift}R_{1c}$ |
| 0.0045 | 347.4707 | 159.2819 | -79.5816 | -41.4548 |

$$R_2 = \begin{cases} R_{2d}, & I \geq 0 \text{ (discharge)} \\ R_{2c}, & I < 0 \text{ (charge)} \end{cases}$$

$$R_{2*} = (R_{20*} + R_{21*}(SOC) + R_{22*}(SOC)^2) \exp\left(\frac{T_{ref}R_{2*}}{T_m}\right) \quad (20)$$

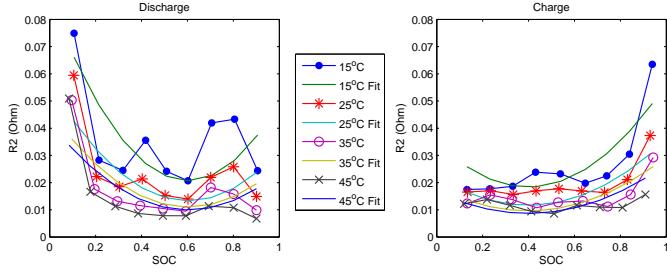


Figure 12. CALCULATED R_2 VERSUS PARAMETRIC FUNCTIONS DESCRIBING THEIR DEPENDENCE ON TEMPERATURE AND SOC.

Table 4. PARAMETRIC R_2 FUNCTION PARAMETERS.

| R_{20d} | R_{20c} | R_{21d} | R_{21c} |
|-----------|-----------|-----------------|-----------------|
| 0.0288 | 0.0113 | -0.073 | -0.027 |
| R_{22d} | R_{22c} | $T_{ref}R_{2d}$ | $T_{ref}R_{2c}$ |
| 0.0605 | 0.0339 | 16.6712 | 17.0224 |

$$C_1 = \begin{cases} C_{1d}, & I \geq 0 \text{ (discharge)} \\ C_{1c}, & I < 0 \text{ (charge)} \end{cases} \quad (21)$$

$$C_{1*} = C_{10*} + C_{11*}(SOC) + C_{12*}(SOC)^2 + (C_{13*} + C_{14*}(SOC) + C_{15*}(SOC)^2)T_m$$

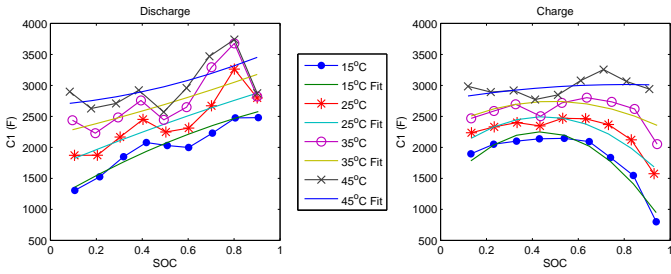


Figure 13. CALCULATED C_1 VERSUS PARAMETRIC FUNCTIONS DESCRIBING THEIR DEPENDENCE ON TEMPERATURE AND SOC.

Table 5. PARAMETRIC C_1 FUNCTION PARAMETERS.

| C_{10d} | C_{10c} | C_{11d} | C_{11c} |
|------------|------------|-----------|-----------|
| 335.4518 | 523.215 | 3.1712e+3 | 6.4171e+3 |
| C_{12d} | C_{12c} | C_{13d} | C_{13c} |
| -1.3214e+3 | -7.5555e+3 | 53.2138 | 50.7107 |
| C_{14d} | C_{14c} | C_{15d} | C_{15c} |
| -65.4786 | -131.2298 | 44.3761 | 162.4688 |

$$C_2 = \begin{cases} C_{2d}, & I \geq 0 \text{ (discharge)} \\ C_{2c}, & I < 0 \text{ (charge)} \end{cases} \quad (22)$$

$$C_{2*} = C_{20*} + C_{21*}(SOC) + C_{22*}(SOC)^2 + (C_{23*} + C_{24*}(SOC) + C_{25*}(SOC)^2)T_m$$

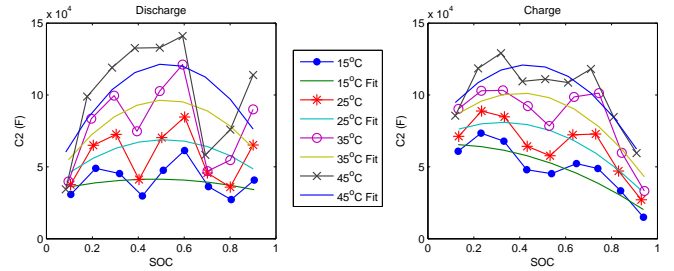


Figure 14. CALCULATED C_2 VERSUS PARAMETRIC FUNCTIONS DESCRIBING THEIR DEPENDENCE ON TEMPERATURE AND SOC.

Table 6. PARAMETRIC C_2 FUNCTION PARAMETERS.

| C_{20d} | C_{20c} | C_{21d} | C_{21c} |
|-----------|-----------|------------|------------|
| 3.1887e+4 | 6.2449e+4 | -1.1593e+5 | -1.055e+5 |
| C_{22d} | C_{22c} | C_{23d} | C_{23c} |
| 1.0493e+5 | 4.4432e+4 | 60.3114 | 198.9753 |
| C_{24d} | C_{24c} | C_{25d} | C_{25c} |
| 1.0175e+4 | 7.5621e+3 | -9.5924e+3 | -6.9365e+3 |